Supplement of Atmos. Chem. Phys., 24, 5117–5147, 2024
https://doi.org/10.5194/acp-24-5117-2024-supplement

Atmospheric Chemistry and Physics
Open Access

Supplement of

Cloud response to co-condensation of water and organic vapors over the boreal forest

Liine Heikkinen et al.

Correspondence to: Liine Heikkinen (liine.heikkinen@aces.su.se) and Ilona Riipinen (ilona.riipinen@aces.su.se)

Supplementary tables

Table S.1 Observation-based input data used in the PARSEC-UFO simulations.

ID	Time [EET]	N_1 [cm^{-3}]	D_1 [nm]	σ_1	N_2 [cm^{-3}]	D_2 [nm]	σ_2	f_{Org}	T [K]
1	11-Apr-2014 18:19:42	165	17	1.92	801	78	1.90	0.66	275
2	12-Apr-2014 15:13:20	2786	38	1.75	72	154	1.75	0.63	281
3	12-Apr-2014 16:50:19	2591	41	1.75	143	150	1.75	0.78	282
4	12-Apr-2014 18:27:45	2233	46	1.75	158	141	1.75	0.72	281
5	13-Apr-2014 13:52:58	427	42	1.79	403	112	1.79	0.54	277
6	13-Apr-2014 17:06:58	574	37	1.75	531	125	1.75	0.50	277
7	13-Apr-2014 18:43:23	681	39	1.77	502	132	1.68	0.49	277
8	14-Apr-2014 14:07:53	2071	33	1.73	44	175	1.72	0.68	279
9	14-Apr-2014 15:44:53	2019	36	1.71	44	168	1.70	0.58	277
10	14-Apr-2014 18:58:22	1445	25	1.82	533	81	1.83	0.73	276
11	15-Apr-2014 14:22:27	320	18	1.81	100	108	1.67	0.41	277
12	15-Apr-2014 15:59:27	2490	11	1.64	130	121	1.72	0.36	275
13	15-Apr-2014 17:36:27	7831	11	1.56	178	92	1.82	0.26	274
14	16-Apr-2014 13:01:04	4019	12	1.68	199	114	1.83	0.53	279
15	16-Apr-2014 16:15:04	7147	17	1.71	95	141	1.75	0.60	274
16	16-Apr-2014 17:52:27	6445	18	1.74	115	130	1.77	0.56	273
17	17-Apr-2014 13:10:21	573	14	1.93	2432	75	1.77	0.49	285
18	17-Apr-2014 14:53:01	1098	9	1.67	1665	75	1.77	0.47	280
19	23-Apr-2014 15:42:18	10036	16	1.58	69	159	1.68	0.35	273
20	23-Apr-2014 17:24:05	8471	18	1.5	81	153	1.67	0.60	272
21	24-Apr-2014 15:42:05	8264	15	1.77	1445	74	1.87	0.74	275
22	24-Apr-2014 17:24:22	2461	24	1.61	1868	67	1.92	0.71	273
23	25-Apr-2014 13:47:46	160	7	1.87	1788	85	1.75	0.75	277
24	25-Apr-2014 17:09:13	469	13	1.64	1760	89	1.75	0.75	276
25	26-Apr-2014 13:32:08	606	12	1.76	1717	111	1.71	0.83	284
26	26-Apr-2014 16:55:49	776	13	1.75	1647	115	1.70	0.81	281
27	26-Apr-2014 18:38:37	862	13	1.75	1611	117	1.70	0.81	281
28	27-Apr-2014 13:20:13	1799	15	1.74	1225	138	1.66	0.74	286
29	27-Apr-2014 15:02:01	1884	16	1.73	1190	139	1.66	0.73	280
30	27-Apr-2014 16:44:19	1970	16	1.73	1155	141	1.66	0.73	278
31	28-Apr-2014 18:31:15	3262	19	1.71	622	170	1.61	0.63	278
32	29-Apr-2014 18:53:44	4484	23	1.69	118	197	1.56	0.54	273
33	30-Apr-2014 15:40:55	586	22	2.03	260	134	1.64	0.31	271
34	30-Apr-2014 17:22:36	486	27	1.95	259	132	1.78	0.25	272
35	01-May-2014 13:47:51	746	20	1.74	321	110	1.75	0.33	272
36	01-May-2014 15:29:30	669	24	1.75	328	112	1.74	0.35	271
37	01-May-2014 18:54:09	527	30	1.75	325	119	1.69	0.34	271
38	02-May-2014 15:17:34	3970	14	2.01	254	85	1.91	0.45	273
39	02-May-2014 16:59:49	3460	16	1.85	305	82	1.83	0.59	272
40	03-May-2014 13:56:25	2481	10	1.73	423	77	1.94	0.57	272
41	03-May-2014 15:38:24	4645	13	1.67	149	114	1.79	0.50	272
42	03-May-2014 17:16:28	5291	17	1.63	150	127	1.71	0.57	272
43	04-May-2014 13:05:10	3135	31	1.63	199	173	1.51	0.66	273
44	04-May-2014 16:34:44	3015	30	1.66	214	170	1.52	0.65	277
45	04-May-2014 18:11:22	2960	30	1.67	221	169	1.53	0.65	278
46	07-May-2014 16:09:31	4293	14	1.69	742	108	1.75	0.49	277
47	07-May-2014 17:50:43	1892	16	1.69	619	113	1.73	0.47	278
48	08-May-2014 14:35:16	820	32	1.81	680	117	1.85	0.48	280
49	08-May-2014 16:17:02	1025	35	1.76	608	122	1.79	0.50	282
50	09-May-2014 16:04:53	478	45	1.79	827	148	1.78	0.72	281
51	09-May-2014 17:47:14	549	50	1.77	677	166	1.81	0.72	283
52	10-May-2014 13:44:17	378	25	1.74	745	101	1.80	0.67	280

53	10-May-2014 15:26:11	395	15	1.67	854	93	1.78	0.73	281
54	10-May-2014 17:14:48	599	13	1.60	969	90	1.73	0.74	282
55	11-May-2014 13:37:10	235	50	1.75	719	95	1.75	0.71	279
56	11-May-2014 17:01:29	542	53	1.75	560	104	1.75	0.67	277
57	11-May-2014 18:43:21	865	59	1.75	416	117	1.75	0.68	276
58	12-May-2014 15:44:33	214	19	1.84	619	91	1.80	0.70	276
59	13-May-2014 15:37:06	462	20	1.95	402	110	1.73	0.79	279
60	13-May-2014 17:18:29	248	24	2.07	365	115	1.73	0.83	277
61	14-May-2014 13:43:03	12316	14	1.67	221	143	1.68	0.52	282
62	14-May-2014 15:25:03	11628	16	1.61	110	181	1.58	0.57	283
63	14-May-2014 18:49:05	9930	18	1.51	95	167	1.59	0.28	286
64	15-May-2014 15:26:25	2487	32	1.88	104	117	1.85	0.57	287
65	15-May-2014 17:06:08	2664	27	2.01	394	83	1.91	0.53	291
66	15-May-2014 18:47:51	1933	26	1.82	622	94	1.79	0.47	293
67	16-May-2014 13:49:12	1588	43	2.04	1158	63	1.36	0.68	289
68	16-May-2014 15:30:49	1346	37	1.94	1397	69	1.47	0.68	292
69	16-May-2014 18:55:09	858	25	1.76	1879	83	1.68	0.69	295
70	17-May-2014 15:19:39	2445	14	1.78	1720	72	1.79	0.75	291
71	17-May-2014 17:00:54	4490	23	1.78	994	93	1.76	0.77	292
72	17-May-2014 18:43:24	6780	29	1.75	215	143	1.69	0.72	292
73	18-May-2014 13:25:36	6098	16	1.75	1277	100	1.74	0.74	289
74	18-May-2014 15:08:34	5917	21	1.75	1361	100	1.75	0.81	288
75	18-May-2014 18:32:48	1491	31	1.74	1923	90	1.76	0.84	288
76	20-May-2014 13:19:50	568	26	2.05	2217	89	1.95	0.70	291
77	20-May-2014 16:59:04	1489	61	1.79	1126	122	1.93	0.73	295
78	20-May-2014 18:30:32	1780	71	1.79	937	108	2.06	0.70	291
79	21-May-2014 13:17:01	724	56	1.76	979	141	1.67	0.65	288
80	22-May-2014 16:06:24	592	31	1.82	1480	131	1.71	0.82	287
81	22-May-2014 17:49:18	790	22	1.75	1454	112	1.75	0.78	282
82	24-May-2014 15:41:37	274	20	2.08	1820	139	1.61	0.76	276
83	24-May-2014 17:44:58	162	16	2.08	1823	138	1.63	0.71	277
84	25-May-2014 13:54:19	849	36	2.08	2309	112	1.82	0.74	276
85	25-May-2014 17:18:08	1246	33	1.76	1743	112	1.73	0.70	278
86	26-May-2014 13:42:24	1755	29	1.93	664	101	1.71	0.82	279
87	26-May-2014 15:24:24	1578	24	2.06	845	73	1.76	0.79	279
88	26-May-2014 17:06:25	1307	26	1.99	688	86	1.75	0.72	281
89	27-May-2014 13:30:45	1828	16	1.68	156	141	1.72	0.49	287
90	27-May-2014 16:54:32	691	22	1.90	177	148	1.74	0.58	286
91	27-May-2014 18:36:31	651	27	1.82	181	164	1.70	0.52	285
92	28-May-2014 13:18:47	2129	47	1.75	45	202	1.75	0.72	283
93	28-May-2014 15:00:47	1909	46	1.92	330	128	1.46	0.74	283
94	28-May-2014 16:42:47	1544	39	2.01	755	65	1.33	0.72	282
95	29-May-2014 13:07:10	1113	59	1.75	116	162	1.75	0.83	283
96	29-May-2014 16:30:59	1014	66	1.75	105	162	1.75	0.83	282
97	29-May-2014 18:12:59	883	67	1.66	311	147	1.78	0.83	284

Table S.2 Overview of ammonium sulfate mass fractions (f_{AS}) used in PARSEC-UFO simulations (first row), and the mass fractions obtained using an ion pairing method (Äijälä et al., 2017 supplementary material). The mass fractions of sulfuric acid (f_{SA}), ammonium bisulfate (f_{ABS}) and ammonium nitrate (f_{AN}) are also provided. The ion pairing calculations are not performed when the ammonium concentrations from the ACSM were negative. These cases are also excluded from the PARSEC-UFO input data for the comparison displayed in this table. It is important to note that these numbers should not be taken as representative values of f_{SA}, f_{ABS} or f_{AS} for the BAECC campaign, because negative ammonium concentrations, which represent noise below the ammonium detection limit, are omitted. In addition, for more reliable estimates of the ion pairing, more sophisticated thermodynamic modeling is required.

Method	Parameter	Min	Max	Median
$f_{AS} = 1 - f_{Org}$ [a]	f_{AS}	0.16	0.75	0.32
Ion pairing	f_{AS}	0	0.73	0.15
	f_{ABS}	0	0.52	0.12
	f_{SA}	0	0.26	0
	$f_{AS} + f_{ABS} + f_{SA}$	0.12	0.75	0.29
	f_{AN}	0	0.17	0

[a] Used in PARSEC-UFO simulation input preparation.

Supplementary figures

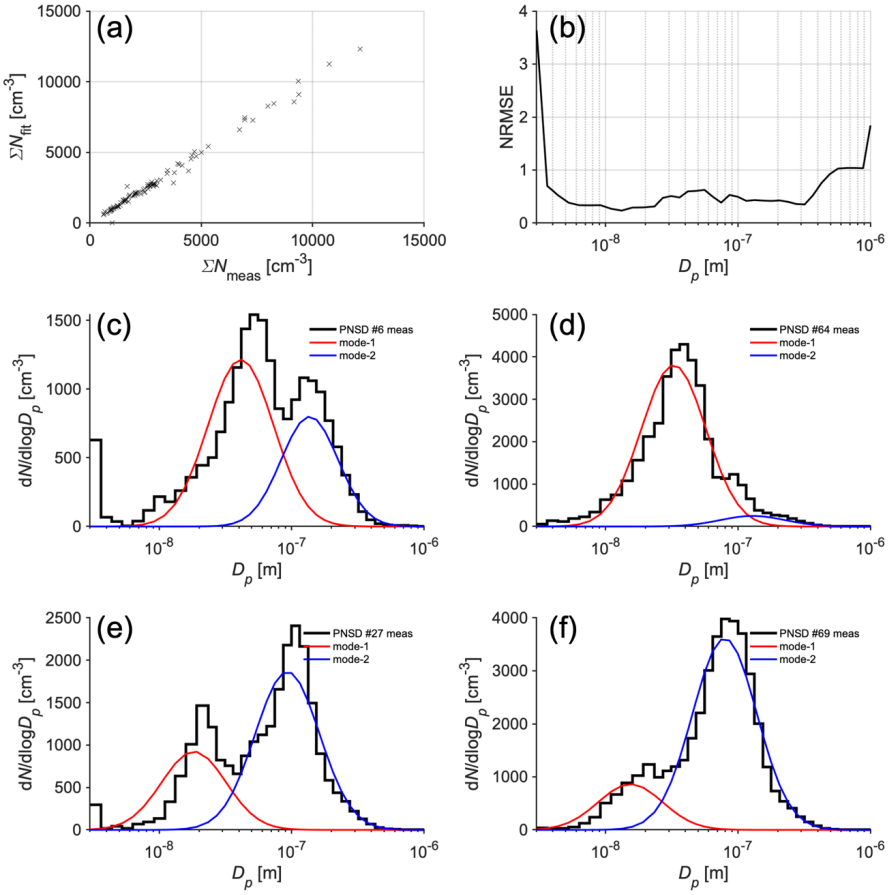

Figure S.1 (a) A scatter plot between the number concentration of aerosol particles retrieved from the bimodal fits (y-axis) and the original DMPS measurements (x-axis). (b) The normalized root mean squared error (NRMSE) as function of particle dry diameter for the bimodal fits. (c–f) Bimodal fit examples are drawn over the observed black PNSD.

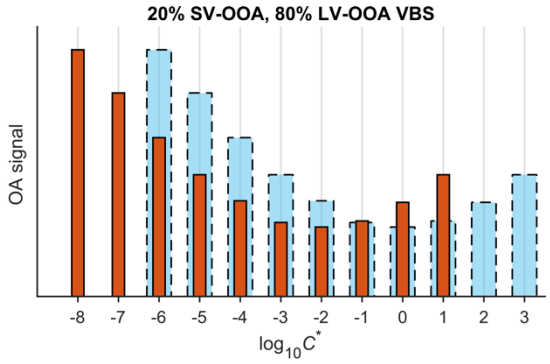

Figure S.2 A volatility basis set representing 20% SV-OOA and 80% LV-OOA. The blue dashed bars represent the volatility distribution under 298K and the red bars represent the BAECC PARSEC-UFO initialization temperature mean: 280K. The $\log_{10}C^*$ axis is shifted according using Eq. (13) found in the main text of the paper. A constant enthalpy of vaporization is used for this example, but in the construction of CJ and F volatility distributions, enthalpy of vaporization depends on $\log_{10}C^*$ (298K; Eq. 17).

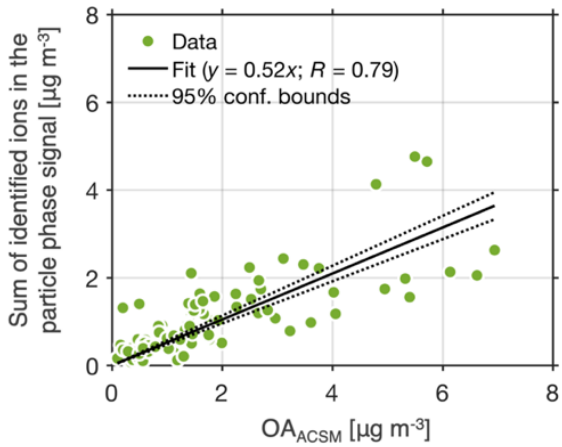

Figure S.3 A comparison between the FIGAERO-I-CIMS particle phase (sum of signals of identified ions in the particle phase) and the OA concentration measured with the ACSM. The data shown here are daytime values only (hour of day >9 and <19) during the BAECC campaign.

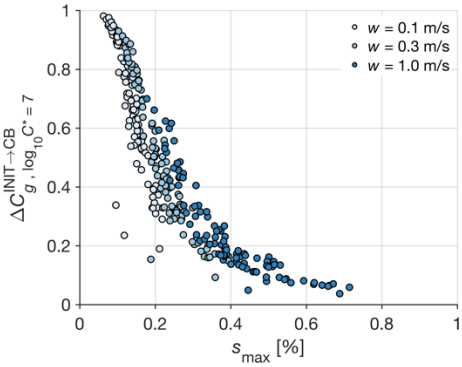

Figure S.4 The fraction of organic vapor (in the $\log_{10}C^*$=7 volatility bin) condensed before the air parcel has reached cloud base vs the maximum supersaturation gained during the ascent. The darkest markers indicate simulations performed with an updraft velocity of 1.0 m s^{-1}, the light blue markers correspond the updraft velocity of 0.3 m s^{-1} and the white markers the updraft velocity of 0.1 m s^{-1}. If a high maximum supersaturation is reached, the condensation sink is low, and less IVOCs condense. If the maximum supersaturation is high, the condensation sink is high, and more IVOCs condense.

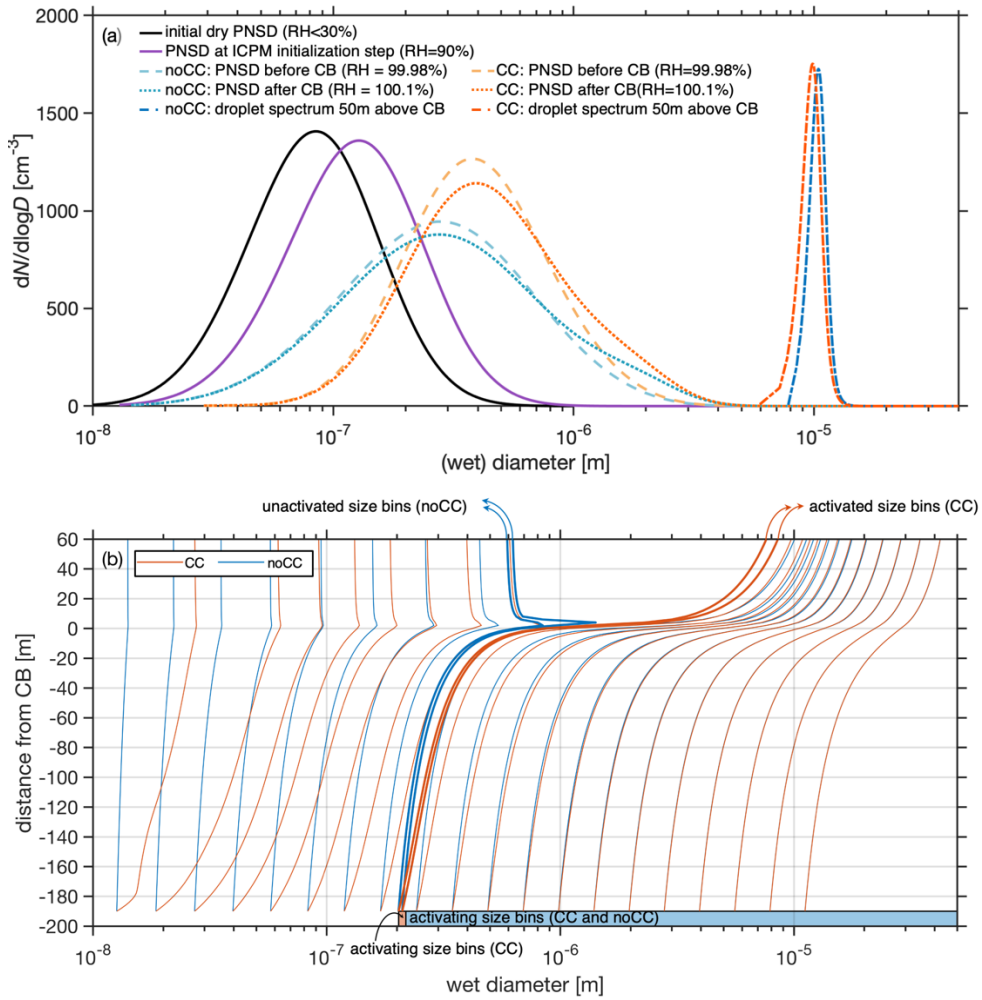

Figure S.5 (a) The evolution of the particle number size distribution (PNSD) during the May 11th case is shown in Fig. 3. The size distributions are obtained from the simulations using a 0.1 m s^{-1} updraft velocity. Red/orange lines correspond to simulations with co-condensation (CC; F volatility distribution) and blue lines simulations without co-condensation (noCC). **(b)** The evolution of the parcel model bin sizes (wet diameter; x-axis) as a function of altitude with respect to cloud base (CB; y-axis). The data shown correspond to the simulation shown in panel (**a**). The bin sizes grow below the cloud base more in the co-condensation simulations which makes the red/orange and blue lines drift as a function of altitude. The bolded curves show the evolution of size bins corresponding to the range from the smallest activated dry radii with CC (r^*_{CC}=66.0 nm) to that modeled when CC is turned off (r^*_{noCC}=71.9 nm). In this range size bins activate only when CC is turned on (small red/orange shaded area at the very bottom of the figure). This results in activation of 4 more size bins as opposed to simulations where CC is turned off. Within the blue shaded area, all size bins activate. The figure composes every 20th size bin out of the 400 bins included in the simulations. Within the red shaded size range, every 2nd bin is displayed with bolded lines.

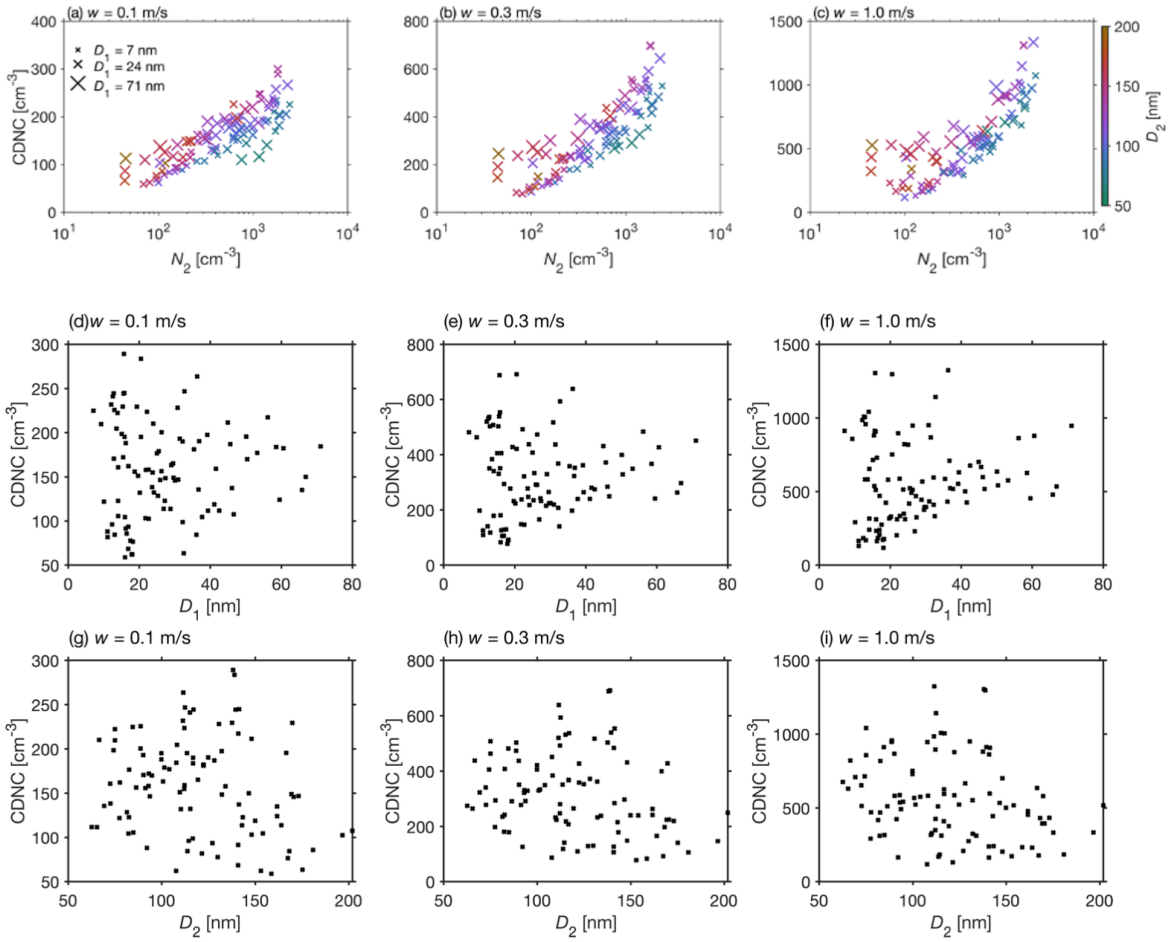

Figure S.6 The relationship between cloud droplet number concentration (CDNC; y-axis) and accumulation mode number concentration (N_2; x-axis), accumulation mode geometric mean diameter (D_2; color-coding), and Aitken mode geometric mean diameter (D_1; marker size) for the 0.1, 0.3 and 1.0 m s^{-1} updraft scenarios, respectively (panels **a–c**) during BAECC. CDNC is obtained from simulations without co-condensation (noCC). N_2, D_2, and D_1 are used as model input data and represent the bimodal fits performed on the measured PNSD using the fitting algorithm by Hussein et al. (2005). Panels d–f and g–i show CDNC vs D_1 and D_2, respectively, for the different updraft velocities respectively.

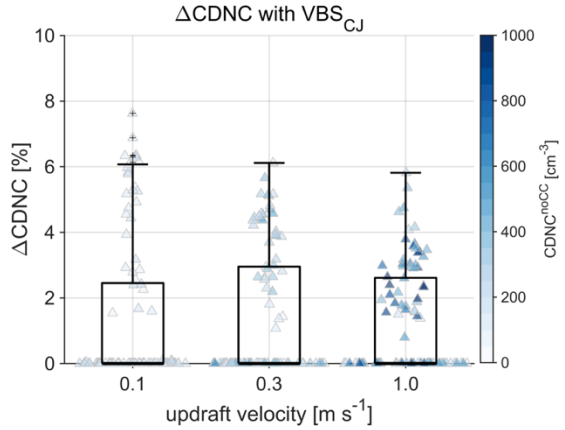

Figure S.7 Box plots showing the predicted ΔCDNC (using CJ volatility distributions) due to co-condensation in the three different modelling scenarios (0.1, 0.3 and 1.0 m s^{-1} updrafts). The colored markers represent CDNC (without accounting for co-condensation) in form of a swarmplot.

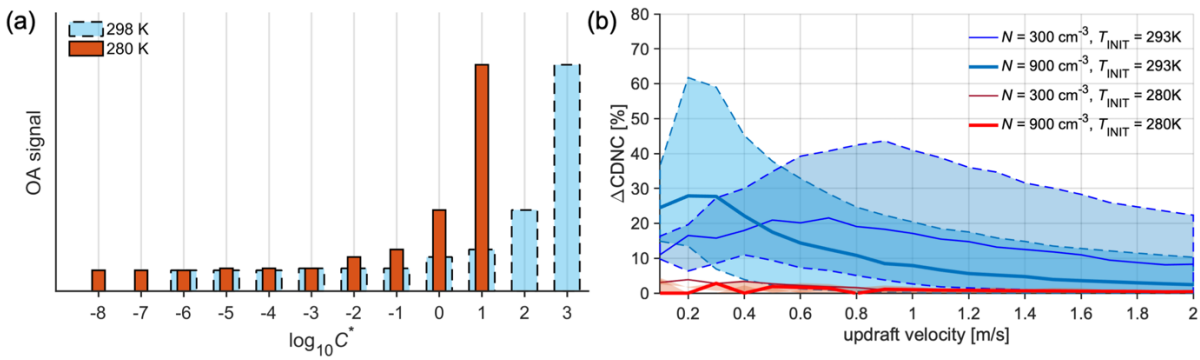

Figure S.8 (a) The volatility basis set shown in Topping et al. (2013) under their reported initialization temperature (light blue) and under the mean BAECC initialization temperature (in red). The $\log_{10}C^*$ axis is shifted according using Eq. (13) found in the main text of the paper. (b) Impact of initialization temperature on Figure 3 in Topping et al. (2013) using an initialization RH of 80%. High CDNC enhancements due to co-condensation using the blue volatility distribution is modeled for clean and polluted cases, and agreement with Topping et al. (2013) is found. When utilizing the temperature-adjusted volatility distribution, and initialization temperature of 280 K, and initialization RH of 80% no significant CDNC enhancements are modeled.

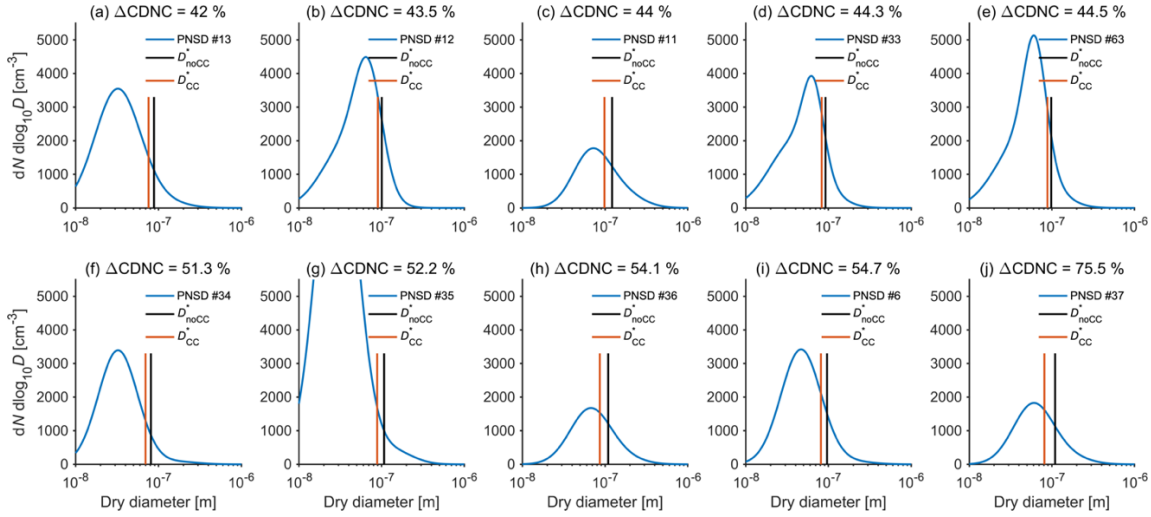

Figure S.9. The different panels show the initial dry PNSD (in blue) for the 10 simulations yielding the highest CDNC enhancements due to co-condensation. The smallest activated dry diameters for simulations without co-condensation (D^*_{noCC}) are highlighted with the black vertical lines, and the smallest activated dry diameters with co-condensation enabled (D^*_{CC}) are shown with the red/orange vertical lines.

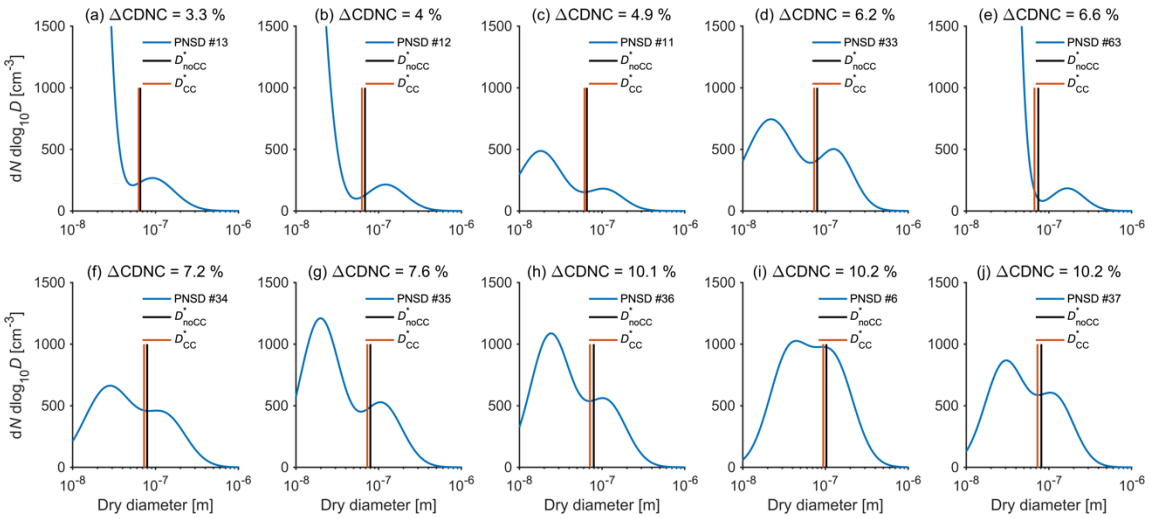

Figure S.10 The different panels show the initial dry PNSD (in blue) for the 10 simulations yielding the lowest CDNC enhancements due to co-condensation. The smallest activated dry diameters for simulations without co-condensation (D^*_{noCC}) are highlighted with the black vertical lines, and the smallest activated dry diameters with co-condensation enabled (D^*_{CC}) are shown with the red/orange vertical lines.

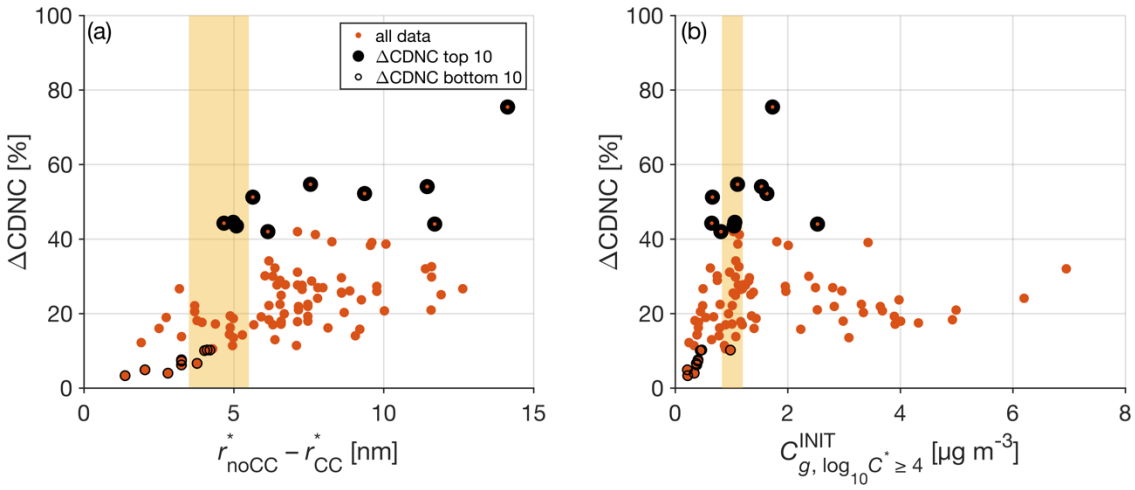

Figure S.11. (a) The relationship between the modeled ΔCDNC and the reduction in the smallest activated dry diameters. All the simulations are shown with the red/orange markers, and the top 10 ΔCDNC are highlighted with the thick black marker edges, and the bottom 10 ΔCDNC with the thin black edges. **(b)** The relationship between ΔCDNC and the initial organic vapor concentration within the $\log_{10}C^*$ range from -4 to 4 ($C^{\mathrm{INIT}}_{g,\ -4:4}$). The ~similar ranges in the reduction of smallest activated dry radii, and $C^{\mathrm{INIT}}_{g,\ -4:4}$ for the bottom 10 ΔCDNC and the top 10 ΔCDNC are highlighted in yellow demonstrating the significantly different ΔCDNC resulting from the varying PNSD shapes between the two groups.

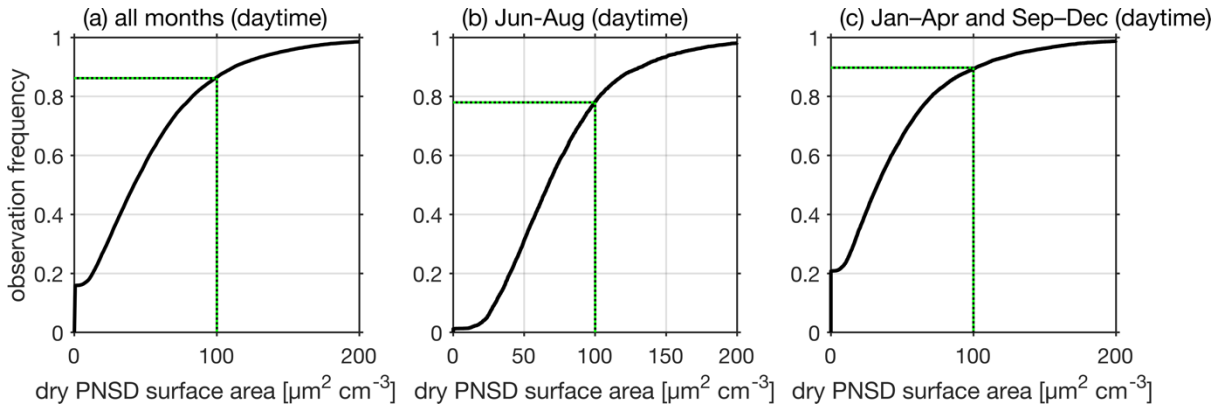

Figure S.12 Cumulative density functions of the dry PNSD surface area calculated from the 2012–2017 SMEAR II DMPS data. Panel **a** contains all the data, panel **b** the summer months and panel **c** the months outside summer. The green lines depict the 100 μm^2 cm^{-3} threshold and the frequencies to which the calculated surface areas remain below the threshold (86% of the time in panel **a**, 78% of the time in panel **b** and 90% of the time for panel **c**).

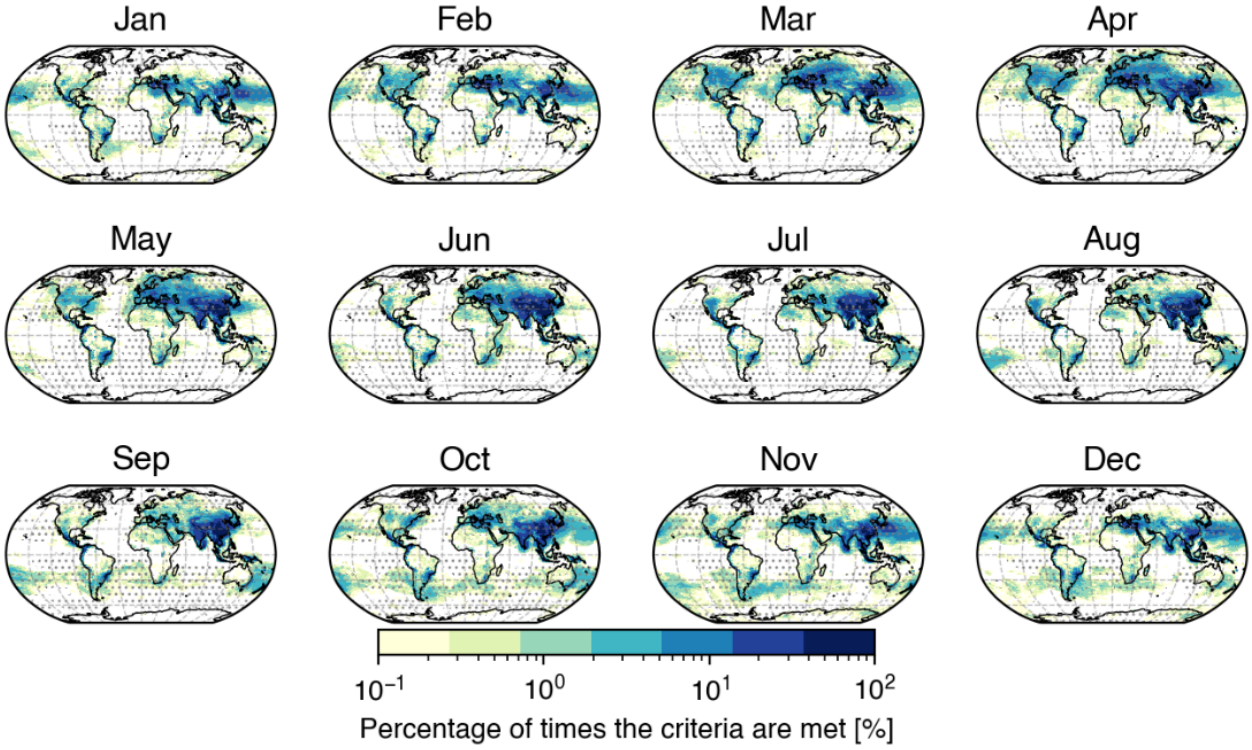

Figure S.13 A global picture of the percentage of times the criteria are met in a 2009–2013 UKESM1 simulation. D_2, D_1 and N_1 are the modal parameters representing the accumulation mode and Aitken mode parameters. The gray markers refer to boreal grid cells, where the median updraft velocity at cloud base is between 0.2 and 0.5 m s^{-1}. Note the logarithmic axis of the color scale.

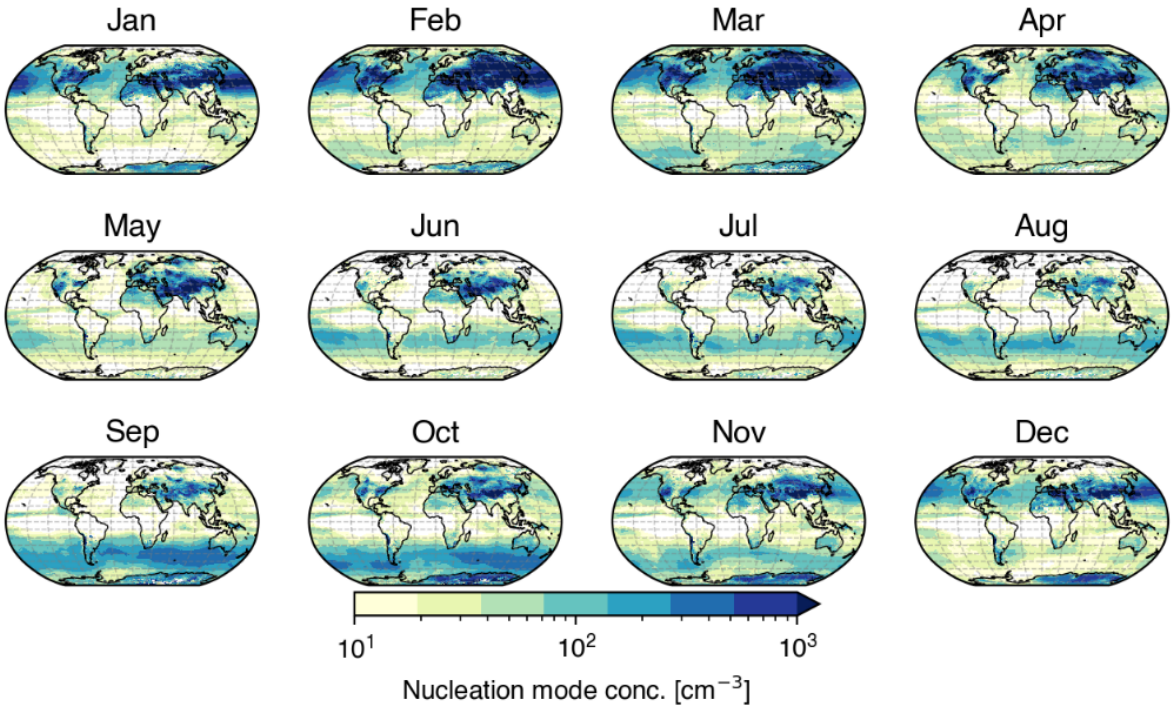

Figure S.14 A global picture of the average daytime concentrations of the nucleation mode in the 2009–2013 UKESM1 simulation. Note the logarithmic axis of the color scale.

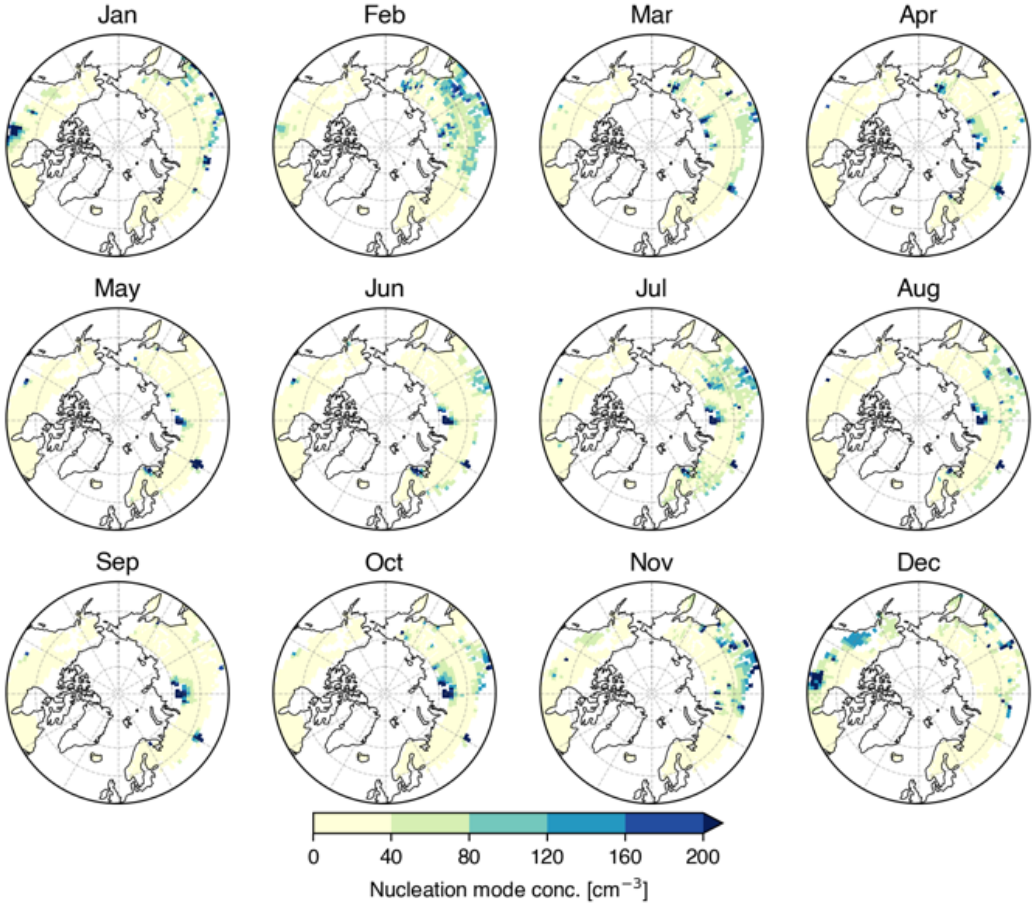

Figure S.15 The average daytime concentrations of the nucleation mode in the 2009–2013 UKESM1 simulation. Only boreal grid cells are shown.

References

Äijälä, M., Heikkinen, L., Fröhlich, R., Canonaco, F., Prévôt, A. S. H., Junninen, H., Petäjä, T., Kulmala, M., Worsnop, D., and Ehn, M.: Resolving anthropogenic aerosol pollution types – deconvolution and exploratory classification of pollution events, Atmospheric Chemistry and Physics, 17, 3165–3197, https://doi.org/10.5194/acp-17-3165-2017, 2017.

Hussein, T., Maso, M. D., Petäjä, T., Koponen, I. K., Paatero, P., Aalto, P. P., Hämeri, K., and Kulmala, M.: Evaluation of an automatic algorithm for fitting the particle number size distributions, Boreal Environ. Res., 10, 19, 2005.

Topping, D., Connolly, P., and McFiggans, G.: Cloud droplet number enhanced by co-condensation of organic vapours, Nature Geosci, 6, 443–446, https://doi.org/10.1038/ngeo1809, 2013.